https://doi.org/10.5194/egusphere-2026-793
Preprint. Discussion started: 17 March 2026

From Snow Depth to Streamflow: Reducing Snowfall Uncertainty in Alpine Headwaters with Sentinel-1 based snow depth retrievals

Shima Azimi[1,4], Manuela Girotto[2], Riccardo Rigon[1], Gaia Roati[1], Silvia Barbetta[3], and Christian Massari[3]

[1]Department of Civil, Environmental and Mechanical Engineering, University of Trento, Trento, Italy
[2]Department of Environmental Science and Policy Management, University of California, Berkeley, California, USA
[3]Research Institute for Geo-Hydrological Protection, National Research Council (CNR), Perugia, Italy
[4]Department of Sustainability and Planning, Aalborg University, Aalborg, Denmark

Correspondence: Christian Massari (christian.massari@cnr.it)

Abstract.

Understanding how the sparse distribution of precipitation gauges at higher elevations contributes to uncertainty in snowfall estimation is crucial in mountainous regions. This is particularly important because uncertainties arising in headwater areas can propagate through hydrological modelling, ultimately affecting the estimation of all components of the water balance. However, establishing dense gauge networks in complex mountain terrain remains challenging, highlighting the value of exploring whether remote sensing observations can help reduce uncertainties in snowfall estimates.

This study assimilates Sentinel-1 C-band snow-depth observations into the snow module of the GEOframe hydrological model, coupled with a snow-density scheme, to update snow depth, snow water equivalent (SWE), and snowfall estimates. The approach is applied to two key Alpine catchments, the Aosta River catchment and the headwaters of the Piemonte catchment in the upper Po River basin, which are critical sources of snowmelt-driven river discharge for sustaining agricultural activities in the Po Valley and have limited high-elevation gauge coverage. Results show that assimilating satellite-derived snow depth increases snowfall estimates across elevation gradients compared to snowfall partitioned by the hydrological model, and substantially improves simulated river discharge during the snowmelt season. Similar improvements are also observed in years without data assimilation, indicating a sustained positive influence on model performance.

1 Introduction

Accurate knowledge about the spatial and temporal distribution of snowfall is essential for managing water resources effectively, supporting agricultural needs and sustaining ecosystems over mountainous regions. Uncertainty in understanding the spatial and temporal patterns of snowfall mainly arises from variability in the magnitude and seasonality of snow–elevation gradients, as well as from landscape characteristics and atmospheric conditions (Harpold et al., 2017; Avanzi et al., 2020; Girotto et al., 2020).

Uncertainties in meteorological forcing data strongly influence snowpack simulation results, particularly limitations in observational networks and forcing data represent a major source of uncertainty in modeling mountain snow patterns (Cho et al., 2022; Raleigh et al., 2016; Lundquist et al., 2019). These uncertainties propagate through snowpack models, leading to significant biases in the simulations (Pflug et al., 2024). The high-quality meteorological input data e.g., precipitation is often scarce in remote or complex terrain. However, precipitation data collected from ground stations remains the most reliable source for quantifying this variable and plays a vital role in meteorological and hydrological studies. These measurements often face challenges due to spatial variability and limited station coverage. Kriging interpolation is a commonly applied geostatistical method for estimating the spatial distribution of ground-based precipitation measurements. Despite its strengths, kriging accuracy decreases in areas where gauge networks are sparse or unevenly distributed, as is commonly the case for mountainous regions. Moreover, kriging tends to smooth out spatial variability, potentially leading to underestimation of localized intense precipitation events (Yamamoto, 2005).

Global and semi-global satellite precipitation products are important sources of precipitation, providing wide spatial coverage, especially in regions with sparse ground-based observations (e.g., Ashouri et al., 2014; Funk et al., 2015; Hou et al., 2014; Hersbach et al., 2020; Gelaro et al., 2017; Dee et al., 2011). However, these global datasets frequently exhibit notable biases compared to ground-based observations. Reanalysis products, which are commonly used as meteorological forcing in models, tend to underestimate precipitation, especially in mountainous regions. This underestimation arises because reanalysis systems have limited ability to capture orographic effects, leading to systematic precipitation deficits in complex terrain (Cho et al., 2022).

Earth observations data supply information on several snow-related variables, including snow cover extent, snow depth, snow surface temperature, and albedo. Recently, the C-band Synthetic Aperture Radar (SAR) observations from the Sentinel-1 European Space Agency constellation have shown significant potential for providing high-quality, moderate-resolution snow data, particularly in regions with deep snowpacks (Lievens et al., 2019, 2022). Additionally, radar-based approaches, which utilize volume scattering principles, have been validated in several airborne campaigns and form the basis of various proposed snow monitoring missions. These techniques are particularly valued for their ability to provide high-resolution, global snow coverage across a wide range of snow depths (Rott et al., 2010). However, these measurements typically face challenges related to revisit frequency and spatial resolution, and they are less accurate over deep or wet snow, in complex terrain, and in areas with dense vegetation (Derksen et al., 2014; Foster et al., 2005; Lievens et al., 2019, 2022).

A potential approach to address limitations of both remote sensing observations and snow models is data assimilation, which integrates observations with models, thereby mitigating uncertainties arising from both sources (Girotto et al., 2014; Margulis et al., 2015; Winstral et al., 2019; Girotto et al., 2020; Smyth et al., 2022). In this regard, this study introduces a data assimilation framework aimed at improving snowfall estimates over mountainous regions. Specifically, Sentinel-1 snow depth observations are assimilated into the GEOframe-NewAge hydrological model's snow module, coupled with a snow density module, to update critical model states such as snow depth, snow water equivalent, and snowfall estimates. The analysis focuses on two key alpine catchments in the upper Po River basin, the Aosta Valley and the headwaters of the Piemonte catchment, both characterized by sparse precipitation gauge coverage at higher elevations and serving as the main sources of snowmelt, which feeds river discharge mostly used for irrigation purposes. We validate our snowfall correction method using observed river discharge during the melt season and a leave-one-out approach, and examine how Sentinel-1 data assimilation modifies snowfall estimates relative to the model's original partitioned snowfall.

The structure of the manuscript is as follows: Section 2 provides an overview of the study area and the datasets used. Section 3 describes the hydrological model and the data assimilation workflow implemented in this research. Sections 4.1 presents the results of the data assimilation process used to correct snowfall over the study area, while Section 4.2 focuses on the effect of the corrected snowfall on the simulated river discharge, particularly during the snowmelt season. Section 4.3 discusses the positive implications of the results, as well as the limitations of the proposed snowfall-correction approach. The final section summarizes the conclusions of the study.

2 Study Area and Datasets

2.1 Study area and ground observed data

The mountainous Aosta Valley catchment, shown in Fig. 1(a) and outlined in red, covers an area of 3,263 km^2 and is located at the northwestern edge of the Italian peninsula. It includes the Italian slopes of Monte Bianco (4,809 m), Monte Rosa (4,634 m), Cervino (4,478 m), and Gran Paradiso (4,061 m), making it the highest region in Italy. The area experiences a typical Cold Continental Climate, with short summers and prolonged cold winters, where temperatures can fall to $-20°$ and below $-30°$ at elevations above 2,000 meters. As a typical inner-Alpine valley, Aosta Valley experiences substantial rain shadows, with annual precipitation ranging from 1,600 to 1,800 mm in the southeastern and windward slopes in the northwest to less than 600 mm in the central valley. This significant variation in precipitation, along with steep temperature gradients, contributes to the region susceptibility to droughts and resulting vegetation stress. A ground-based dataset of daily precipitation and temperature measurements from 81 gauges across the Aosta Valley is used for the period 2010–2020 (see gauge locations in Fig. 1(a)). Fig. 1(b) shows the elevation bands within the Aosta catchment along with the number of rain gauges in each band. The figure indicates that most gauges are located below 2,400 meters. While a significant portion of the Aosta catchment lies above 2,400 meters, there are only seven rain gauges in these higher elevation bands. This sparse coverage can introduce substantial bias in precipitation estimates when using interpolation methods such as kriging.

The high-elevation areas of the Piemonte catchment, covering 7,870 km^2 in the western and northern Alps of Italy, generally rise above 1,500 meters and are characterized by substantial snowfall and rugged terrain (see orange border in Fig. 1(a)). Daily precipitation data from approximately 150 gauges, distributed across these high-elevation areas (gauge locations also shown in Fig. 1(a)), were used for the period 2015–2018. Fig. 1(c) presents the elevation bands within the high-elevation areas of the Piemonte catchment, along with the number of rain gauges in each band. Although the number of rain gauges in the highest elevation bands is still limited, gauge coverage is higher than in the Aosta River catchment.

Daily river discharge data from 12 hydrometric stations over the Aosta Valley catchmentnt, covering the period 2010–2020, were used to calibrate model parameters, validate results, and support further analysis. All data were provided by the Regional Functional Center of the Aosta Valley and are available for download at https://cf.regione.vda.it/portaledati.php.

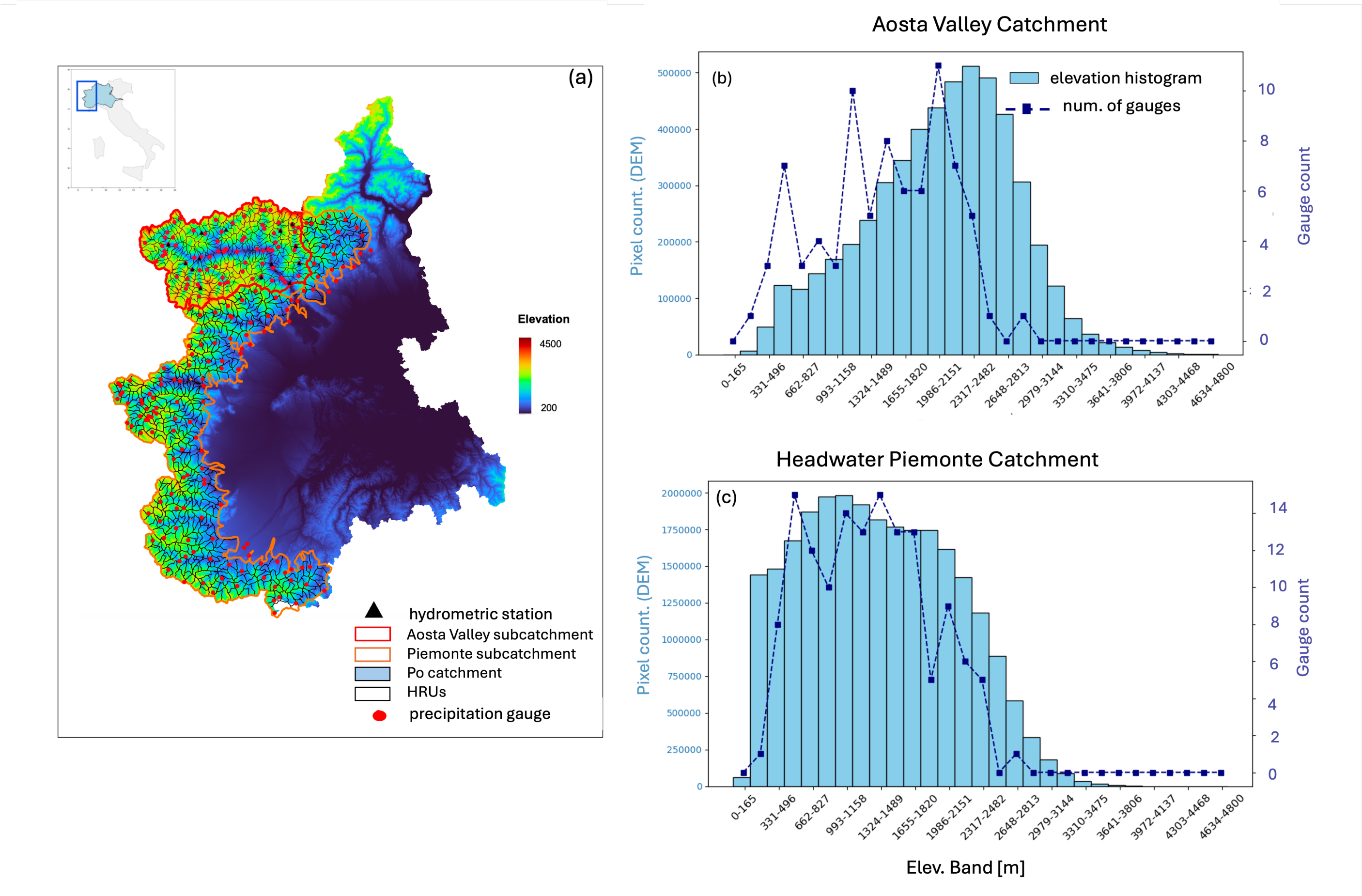

Figure 1. (a) Map of the study area, including the Aosta Valley catchment (red outline) and the high-elevation regions of the Piemonte catchment (orange outline). The area outlined in red represents the Aosta Valley catchment, while the remaining delineated subcatchments correspond to the high-elevation regions of the Piemonte catchment. The headwaters of the Piemonte and Aosta Valley catchments lie within the upstream Alpine sector of the Po River basin. In this study, only the high-elevation sub-catchments of Piemonte are considered, rather than the entire region. The distribution of precipitation gauges across the study area is also shown in the histogram graphics. (b) Histogram showing the elevation distribution and the number of gauges within each elevation band in the Aosta River catchment. (c) Histogram showing the elevation distribution and the number of gauges within each elevation band in the headwater of the Piemonte catchment.

2.2 Sentinel-1 snow depth

We use data from a two-satellite constellation, S1A and S1B, of the Sentinel-1 mission, launched in April 2014 and 2016, respectively. Each satellite follows an exact 12-day repeat cycle, completing 175 orbits within each cycle. Positioned in the same orbital plane with a 6-day phase offset, this dual-satellite setup achieves a precise 6-day repeat cycle. Additionally, depending on the area, more frequent observations (averaging every 2–3 days) are possible due to partly overlapping swaths and the combination of ascending and descending orbital passes (Lievens et al., 2019, 2022). The snow depth retrieval process utilizes the sensitivity of the radar C-band backscatter signal to changes in snow accumulation and melting and it uses a change detection method to derive snow depth values (Lievens et al., 2019). The snow depth algorithm leverages the volume scattering principle caused by the snowpack as a dense medium composed of clustered, irregular ice crystals. Additionally, enhanced scattering can arise from interactions at snow layer interfaces and at the snow-ground boundary. Generally, a deeper snowpack results in more intense scattering, allowing the strength of the scattering signal to be correlated with snow depth (Girotto et al., 2024). The data with 500m spatial resolution is freely downloadable from https://ees.kuleuven.be/project/c-snow for the period from mid-2016 to 2023.

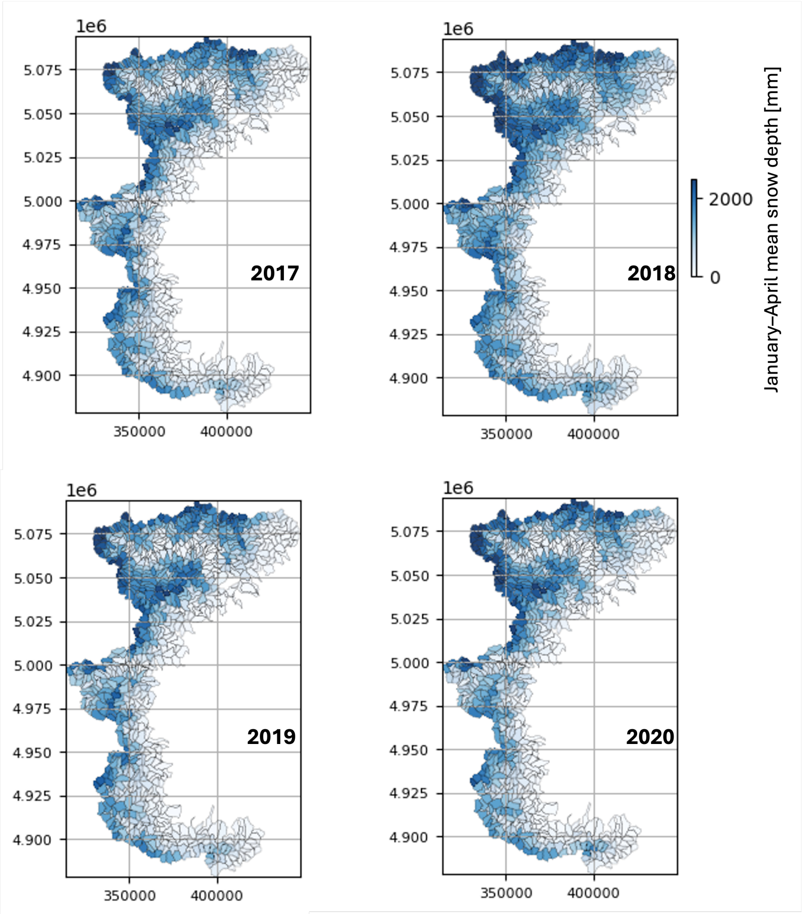

Figure 2. January–April mean snow depth retrieved from Sentinel-1 data during 2017-2020, averaged over subcatchments within the Aosta Valley catchment and the headwater of the Piemonte catchment.

Fig. 2 presents the January-April mean snow depth retrieved from Sentinel-1 data for the water years 2017-2020, averaged over subcatchments within the Aosta Valley catchment and the high-elevation areas of the Piemonte catchment. The figure indicates that a large part of the snow accumulation occurs in the Aosta Valley, with higher snow depths observed in the 2018 and 2020 water years.

3 Methods

3.1 GEOframe-NewAGE hydrological model

The GEOframe-NewAGE modeling system is a semi-distributed hydrological model that integrates different components to simulate various processes within the hydrological cycle. It is developed to manage the complexities of hydrological processes, offering a flexible, modular, and open-source environment (Bancheri et al., 2019; Formetta et al., 2014). The delineation of subcatchments is derived using the Horton Machine toolbox (Abera et al., 2017). Additionally, the Extended Petri Net (EPN) (Bancheri et al., 2019) illustrated in Fig. 3 delineates the allocation of precipitation flux into snowfall and rainfall based on air temperature (Formetta et al., 2014). Subsequently, melted snow augments the liquid water in snow, with options for refreezing or transferring to the vegetation. The input flux into the canopy reservoir either evaporates from the canopy or descends to the soil (Fig. 3(b)). The portion reaching the soil is distributed across three reservoirs, outlined in Fig. 3(c). For a comprehensive understanding of reservoir functionality, readers are encouraged to refer to primary references such as Formetta et al. (2014) and Bancheri et al. (2019). Including the correction factors for rainfall and snowfall (α_r and α_s), the model contains 19 parameters (see Table A1), all of which can be calibrated by the user following a sensitivity analysis.

3.1.1 Snow component in GEOframe-NewAGE

The snow component in GEOframe-NewAge (Formetta et al., 2014) is modeled through two primary steps: separating snowfall and rainfall, and generating meltwater discharge. Rainfall and snowfall are separated using the following equations:

$$P_r = \alpha_r \left(\frac{P}{\pi} \arctan(T - T_m) + \frac{P}{2} \right) \tag{1}$$

$$P_s = \alpha_s (P - P_r) \tag{2}$$

where P_r and P_s represent the rainfall and snowfall components of total precipitation P, respectively. Here, T is the air temperature, T_m is the melting temperature, and α_r and α_s are correction factors of rainfall and snowfall that can be adjusted during calibration.

The snow modeling, including the computation of snow water equivalent and melting discharge, is achieved by solving the following differential equations. For a detailed description of the terms in these equations, please refer to (Formetta et al., 2014).

https://doi.org/10.5194/egusphere-2026-793
Preprint. Discussion started: 17 March 2026

Variables	Description
Snow Component	
P	Precipitatoin
P_r	Rainfall
P_s	Snowfall
R	Frozen water
M	Melted snow
M_d	Melting discharge
SWE	Snow Water Equivalent
W_s	Liquid water in snow
SD	Snow depth
Canopy Component	
Et_c	Actual canopy ET
S_C	Canopy storage
U_1	Fast runoff
U_2	Slow runoff
T_r	Throughfall
Remaining Components	
S_{RZ}	Rootzone storage
S_R	Runoff storage
S_{GW}	Groundwater storage
ET_{RZ}	Actual rootzone ET
R_e	Groundwater recharge
Q_R	Surface runoff
Q_{GW}	Groundwater contribution to runoff
Q_T	Subbasin out runoff

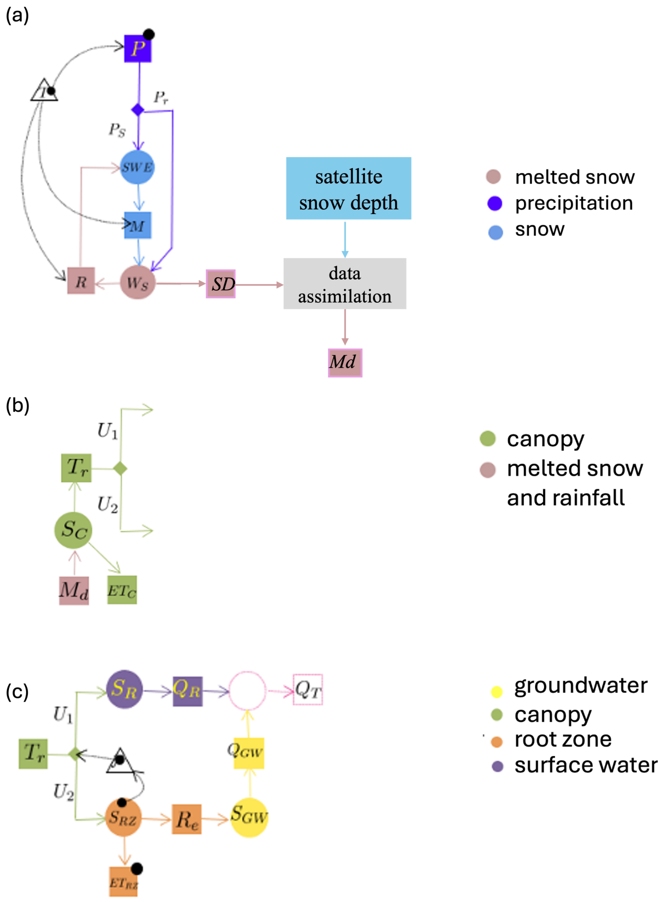

Figure 3. Representation of the water cycle in the GEOframe modeling system, illustrating: (a) the snow reservoir along with satellite-derived snow data assimilated into the model, (b) the canopy layer, and (c) the ground and subground reservoirs.

$$\begin{cases} \frac{dS_r}{dt} & = P_r + m - f - M_d \\ \frac{dS_s}{dt} & = P_s + f - m \\ SWE & = S_s + S_r \end{cases} \tag{3}$$

where m and f represent the melt and freeze water, respectively, and M_d denotes the melting discharge. The sum of the liquid water (S_r) and solid water (S_s) in the snowpack is defined as the snow water equivalent (SWE).

To enable snow depth estimation, a snow density scheme using the iSnobal parameterization (Marks et al., 1999) has been integrated into the GEOframe model. This parameterization, widely adopted by the snow science community, has been validated across various scales and mountain environments (Painter et al., 2016; Hedrick et al., 2018; Girotto et al., 2024).

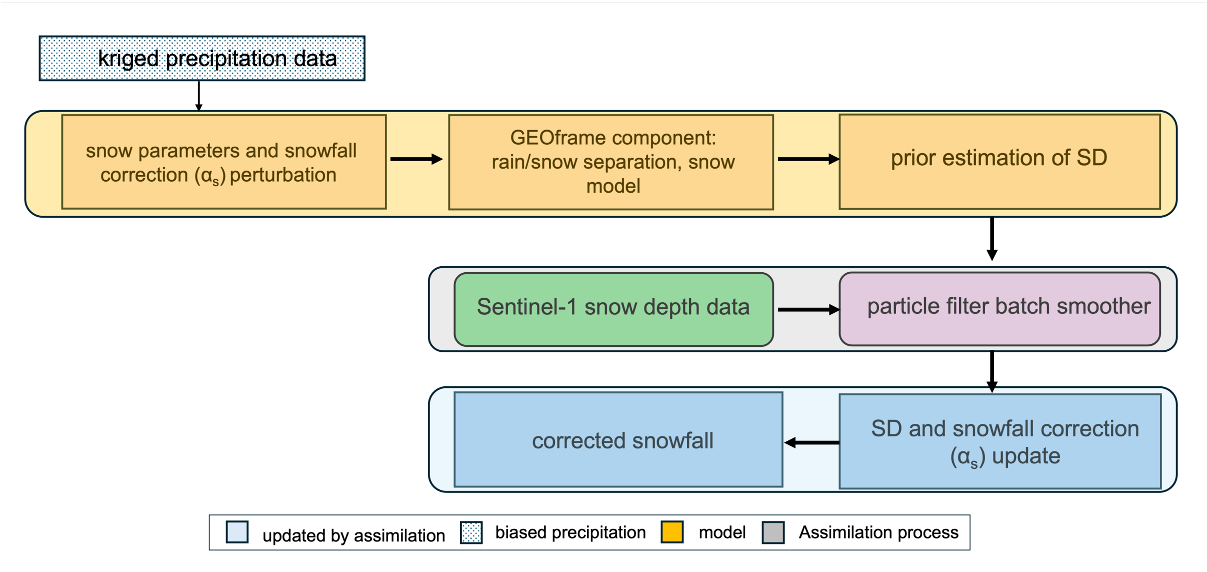

Figure 4. Flowchart to illustrate the methods used to assimilate Sentinel-1 snow depth retrieval with snow depth simulated by GEOframe model. In the flowchart, SD denotes snow depth.

3.2 Particle filter batch smoother

The primary aim of a particle filter is to estimate the unknown state of a system based on a series of noisy observations. Instead of relying on a single estimate, the particle filter employs a set of possible states, known as particles, to approximate the probability distribution of the system state. Each particle represents a potential state, and together they provide an approximation of the system's actual underlying state. Particle filters are well-suited for highly nonlinear systems and can handle non-Gaussian state variables, unlike the Kalman filter, which assumes linearity and Gaussian distributions (Gordon et al., 1993). The particle batch smoother is a particular case of the traditional particle filter that allows for a more refined estimate of the system state by considering all available observations (Leeuwen, 2009). It is useful in situations where a complete understanding of the system state is required over the entire observation period, not just in real-time (Margulis et al., 2015). In following section, we describe the methodology used to assimilate Sentinel-1 snow depth retrievals with snow depth simulated by GEOframe hydrological model. Specifically, we present a particle filter batch smoother to estimate the posterior distribution of snow depth and to adjust the snowfall forcing accordingly (see Fig. 4).

3.2.1 Data assimilation setup in GEOframe model

The core approach follows the method outlined in Girotto et al. (2024), with key differences: here, data assimilation is implemented within the GEOframe hydrological model, focusing specifically on correcting the portion of precipitation classified as snowfall in the model.

- **Ensemble generation**

  In this study, we assume that the primary source of uncertainty in estimating snow depth in mountainous regions is the bias in snowfall estimates, which is accounted for by adjusting the parameter snowfall correction factor (α_s). An ensemble of 100 particles, α_s, is used, as our analysis indicates this number of particles is sufficient to ensure stable performance of the particle filter method. Values for α_s are drawn from a log-normal distribution with a mean and coefficient of variation set to 1. Uncertainty is also attributed to the remaining five snow-related parameters in the model. These are sampled from a normal distribution within predefined ranges specified by the model. Additionally, the rainfall correction factor (α_r) is set to 1. The GEOframe model is run 100 times, with each run incorporating the α_s along with other snow parameters generated during the particle sampling step.

  Before the update step, each particle is assigned an equal probability of occurrence, resulting in weights defined as:

  $$w_j^- = \frac{1}{N_{\text{ens}}} \tag{4}$$

  where $\sum_{j=1}^{N_{\text{ens}}} w_j^- = 1$.

- **Updating the state variables**

  The target of the update step is to adjust the weights of the ensemble particles by assimilating Sentinel-1 snow depth retrievals. The weights are determined by comparing the predicted state of the particle to the observed data. The predicted state here is snow depths obtained by the model and observed data refers to the Sentinel-1 snow depth retrievals. This is achieved by calculating the likelihood function $p(Z|Y)$, where Z is Sentinel-1 snow depth retrievals within the assimilation window, and Y represents the assimilation control vector. In our case, Y consists of the N_{ens} values of snowfall correction factor α_s. The likelihood function corresponds to the specified probability distribution function for observation errors, $p_v(Z - M_j^-)$, where M_j^- denotes the predicted snow depth from particle j (which is snowfall factor j).

  The probability distribution function $p_v(Z - M_j^-)$ is generally represented by a Gaussian process, assuming that observation errors have a zero mean with a specified error covariance, C_v (Eq. 5).

  $$p_v(Z - M_j^-) = \frac{1}{\sqrt{(2\pi)^{N_{\text{obs}}}|C_v|}} \exp\left(-\frac{1}{2}(Z - M_j^-)^T C_v^{-1}(Z - M_j^-)\right) \tag{5}$$

  The updated weights for each particle are computed as follows:

  $$w_j^+ = \frac{C_0}{N_{\text{ens}}} p_v\left(Z - M_j^-\right), \tag{6}$$

  $$C_0 = \frac{N_{\text{ens}}}{\sum_{k=1}^{N_{\text{ens}}} p_v\left(Z - M_j^-\right)} \tag{7}$$

https://doi.org/10.5194/egusphere-2026-793
Preprint. Discussion started: 17 March 2026

where w_j^+ is the updated weight for particle j, C_0 is a integration constant, N_{ens} denotes the ensemble size, and $p_v(Z - M_j^-)$ represents the likelihood of the observation errors. The updated weights provide a discrete approximation of the posterior probability distribution, enabling the estimation of posterior snowfall and snow depth values. Fig. 4 illustrates the process of assimilating modelled snow depth with Sentinel-1 snow depth retrievals to estimate the posterior values of snowfall and snow depth.

- **Data assimilation implementation steps**

  The process of data assimilation for each subcatchment (HRUs) begins by generating the particles, which are the correction factors of snowfall (α_s), after which the snow components of the GEOframe model are run for each correction factor. The other parameters in the snow component of the model, melting temperature, freezing factor, melting factor, radiation factor, and snow porosity, are sampled within their respective allowable ranges to account for parameter uncertainty in the data assimilation process (see Table A1 for the parameter ranges). In addition, the average snow depth retrieved from each subcatchment from Sentinel-1 is incorporated into the assimilation process. Sentinel-1 snow depth data are assimilated only on dates following storm events occurring between January and mid-April, when the likelihood of dry snow conditions is higher. The weights corresponding to particles (α_s) are updated during the "update" phase of the data assimilation based on Eq. 5 and 6. Subsequently, α_s and other snow model parameters, in each subcatchment, are estimated as weighted averages using the updated particle weights.

4 Results and Discussion

In this section, we present the results of assimilating Sentinel-1 snow depth data into the GEOframe model, applied to Aosta River Catchment and the headwater of Piemonte, as a part of the Italian Alps. The general data assimilation framework is first described in Section 4.1. We then present the corrected snowfall obtained using the proposed assimilation method and its evaluation. Subsequently, the modified snowfall are used to simulate river discharge in the Aosta Valley catchment, enabling an assessment of the proposed method effectiveness in reproducing observed streamflow during the snowmelt season (Section 4.2). Finally, Section 4.3 discusses the benefits and limitations of the proposed approach.

4.1 Data assimilation over Aosta Valley and headwater of Piemonte catchments

Given the difficulty of maintaining dense gauge networks in high-elevation terrain, this section evaluates the potential of remote-sensing observations to reduce uncertainty in snowfall estimates at these elevations. In this regard, the potential of the data assimilation approach proposed in Section 3.2.1 is investigated through the incorporation of Sentinel-1 snow depth data into the model. Through a comparison of ground measurements and Sentinel-1 snow depth, the average of the Mean Absolute Error (MAE) is 454.1 ± 216.4 mm for the Aosta Valley catchment.

For the Aosta Valley catchment, the data assimilation is applied over the 2017–2020 water years, corresponding to the period of available Sentinel-1 snow depth observations. Fig. 5 presents that 100 snow depth ensemble members are generated

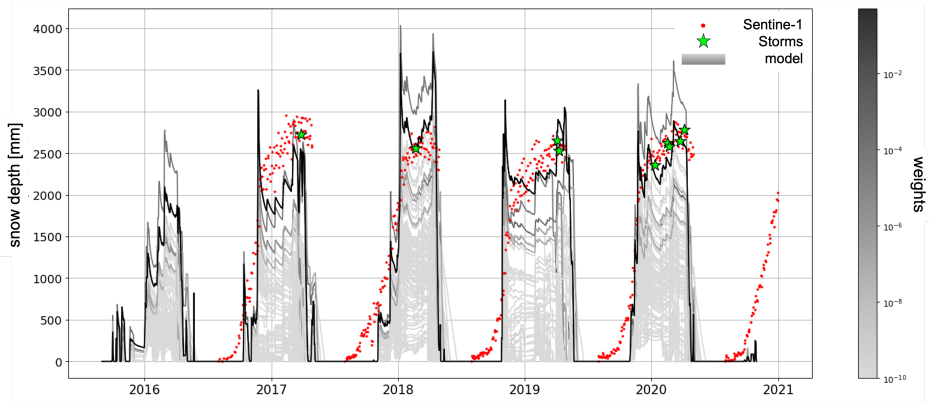

Figure 5. Snow depth ensemble (100 samples) generated based on different particles (snowfall correction factors, α_s). The color scale indicates the updated weights (Eq. 6) of the generated snow depths, with black representing values closer to the posterior snow depth, and light grey indicating values further from it. This plot specifically shows the results for a subcatchment within the Aosta Valley catchment.

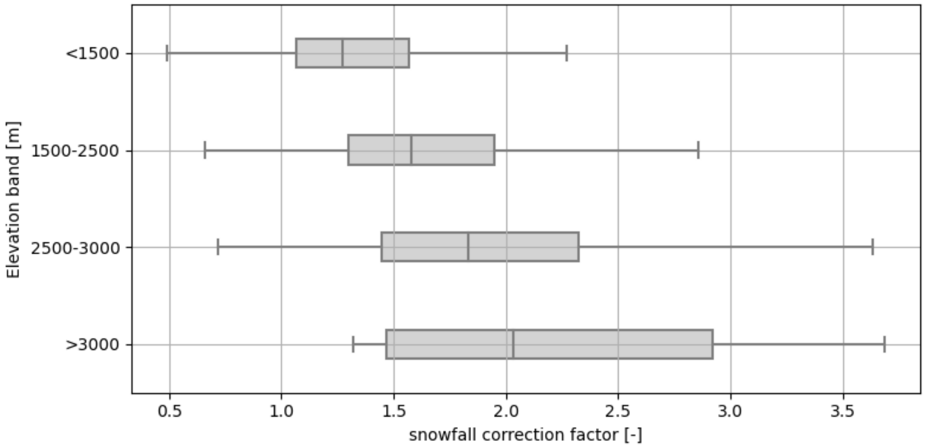

Figure 6. Snowfall correction factor distribution across different elevation bands over the entire study area. Higher correction factors at higher elevation bands indicate increased uncertainty in snowfall estimation by the model compared to lower elevations.

by the model for a subcatchment over the Aosta Valley catchment, each corresponding to a set of α_s and the other perturbed snow model parameters. In this figure, darker colors indicate higher particle weights, reflecting a stronger agreement with the posterior snow depth, while lighter grey colors represent lower weights and a greater deviation from the posterior estimate. The rainfall correction factor (α_r) is fixed at 1, based on the assumption that only snowfall is subject to correction using snow depth observations. Hereafter, rainfall and snowfall with α_r and α_s equal to 1 are referred to as baseline rainfall and baseline snowfall, respectively, and their sum is defined as baseline precipitation. (see Eq. 2). When α_s is instead derived through data assimilation, the resulting snowfall is referred to as corrected snowfall. The distribution of the snowfall correction factor across

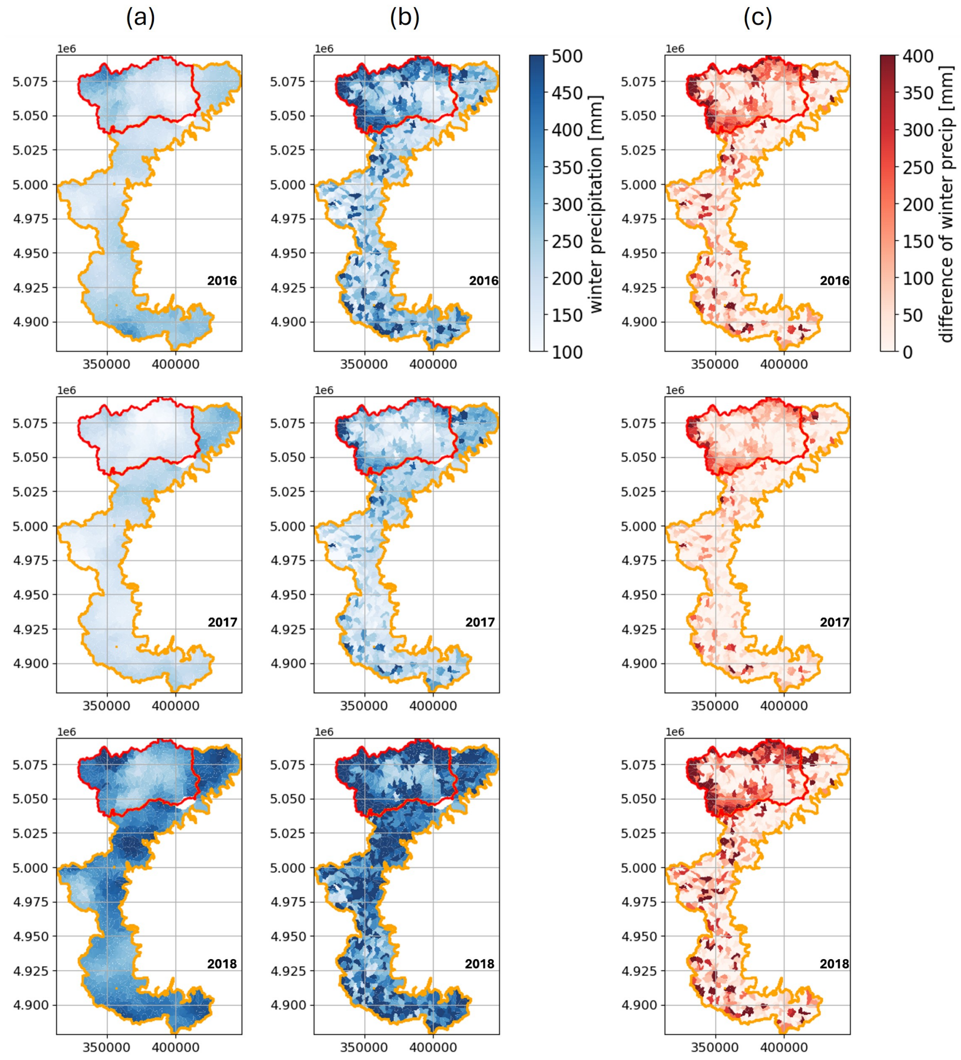

Figure 7. Spatial variation of total precipitation during January-March (snowfall plus rainfall) across the catchment, shown for each sub-catchment, as derived from (a) the kriging interpolation method and (b) after correcting snowfall through the assimilation of Sentinel-1 snow depth data. Panel (c) presents the difference between (a) and (b), highlighting that the largest differences occur at the higher elevations of the Aosta catchment, while differences in the valley areas are minimal. The red border indicates the Aosta River catchment, and the orange border indicates the headwaters of the Piemonte catchment.

elevation bands for the entire study area, shown in Fig. 6, demonstrates that this factor increases with elevation, suggesting that the model increasingly underestimates snowfall at higher elevations and that associated uncertainty grows with elevation.

https://doi.org/10.5194/egusphere-2026-793
Preprint. Discussion started: 17 March 2026

Fig. 7(a) (red border) illustrates the spatial distribution of January–March precipitation across the Aosta Valley catchment during the 2016–2018, showing lower values in the central part of the catchment, which is characterized by lower elevations. Total precipitation in this panel is obtained through interpolation of ground observed precipitation measurements for each subcatchment and corresponds to the sum of the baseline rainfall and snowfall in Eq. 2 (with α_r and α_s both set to 1). Additionally, the winter values (January–March) associated with the total precipitation, calculated as the sum of the corrected snowfall and baseline rainfall during 2016–2018, are shown in Fig. 7(b). The results indicate an increase in total precipitation at higher elevations, primarily due to the enhanced snowfall estimates. Fig. 7(c) shows the difference between panels (a) and (b), allowing visualization of the areas where snowfall has been corrected. The figure indicates that, at lower elevations (the central part of the Aosta Valley), the differences are close to zero, while most of the changes occur at higher elevations (see the red boxes in Fig. 7). Owing to the longer data availability in the Aosta River catchment, the comparison between the corrected and original snowfall for this area is shown separately in Fig. A1. Fig. A1 also demonstrates that the difference between the corrected and baseline snowfall at higher elevations is more pronounced, while it remains close to zero in the low-elevation valley.

The study area is extended to the high-elevation regions of the Piemonte catchment, where Sentinel-1 snow depth retrievals (MAE 398.6 ± 193.6 mm relative to ground measurements) are assimilated into the GEOframe model to improve snowfall estimates. Compared to the Aosta Valley catchment, gauge density is higher across the upper elevation bands. Figure 7(a) (orange outline) shows the January–March total precipitation for each subcatchment for 2016–2018, obtained by interpolation as the sum of baseline snowfall and rainfall. The corresponding panels in Fig. 7(b) show January–March total precipitation after assimilation (corrected snowfall plus baseline rainfall). Unlike the Aosta Valley catchment, baseline and corrected snowfall in the Piemonte catchment differ only slightly across most subcatchments, with generally higher corrected values, as further illustrated in Fig. 7(c) (orange border).

The corrected snowfall over the study area is validated using a leave-one-out approach, in which one precipitation gauge is excluded and its precipitation is first estimated via kriging. Sentinel-1 snow depth from the nearest grid cell is then assimilated to adjust snowfall, and total precipitation is obtained by adding this corrected snowfall to the baseline rainfall. These two estimates are subsequently compared to evaluate the correction performance. Fig. 8 presents the RMSE against observations at the excluded gauge, demonstrating the improvement in winter precipitation (January–March) estimates with data assimilation.

Additionally, a cross-comparison is performed between SWE values derived from the corrected snowfall in the GEOframe model and the IT-SNOW dataset (Avanzi et al., 2022). The correlation coefficients, along with time series comparisons for different elevation bands, are presented in Fig. A3 and Fig. A4 in the Appendix.

4.2 Hydrological modeling over Aosta Valley catchment

In this section, the hydrological model forced with kriged precipitation is referred to as the baseline model, while the model using corrected precipitation values through data assimilation is referred to as the DA-based model. In the baseline model, 17 parameters related to snow, canopy, runoff, root zone, and groundwater components are calibrated using observed river

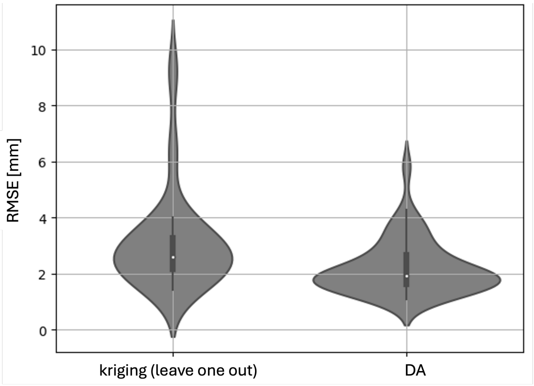

Figure 8. Variation in Root Mean Square Error (RMSE) between observed January–March precipitation and estimates from kriging and data assimilation at gauge locations excluded during leave-one-out validation.

discharge data from 12 hydrometric stations across the Aosta catchment. In this setup, the rainfall and snowfall correction factors, α_r and α_s, are both fixed at 1.

In the DA-based model, snow-related parameters including α_s and the five other parameters described in Section 3.1.1 are estimated through the assimilation of Sentinel-1 snow depth retrievals into the model for the period 2017–2020. For the remaining years within the 2010–2020 period, the same set of snow parameters derived during the assimilation period is applied. The remaining parameters, related to canopy processes, runoff generation, root zone, and groundwater, are calibrated using observed discharge data from 12 hydrometric stations distributed across the catchment over the period 2015–2018 and subsequently validated during the remaining years within the 2010–2020 period. Fig. A2 presents the variation in KGE values between simulated and observed river discharge during the calibration period across the Aosta Valley catchment for both the baseline and DA-based models, highlighting the differences in their performance. The figure demonstrates that assimilating Sentinel-1 snow depth retrievals into the hydrological model enhances its ability to more accurately reproduce observed river discharge. The baseline model results for reproducing river discharge at the catchment outlet yielded KGE scores of 0.72 during the calibration period and 0.71 during the validation period. The DA-based model demonstrates enhanced performance in simulating river discharge at the catchment outlet, achieving improved KGE scores of 0.87 during the calibration period and 0.88 during the validation period (see Fig. 9). Moreover, Fig. 9(a) illustrates that the DA-based model reproduces low flows more accurately than the baseline model, as indicated by the comparison of the red and green time series during periods of low discharge. The flow duration curve in Fig. 9(b) further supports this observation . In addition, the figure shows that the DA-based model provides better estimates of peak and higher flows during spring and summer, when snowmelt occurs, compared to the baseline model. The correlation between observed discharge and that simulated by the DA-based model and the baseline model during spring and summer (periods dominated by snowmelt) is shown in Fig. 10. The results demonstrate a higher correlation for the DA-based model compared to the baseline, indicating that correcting snowfall positively contributes to a more accurate simulation of river discharge.

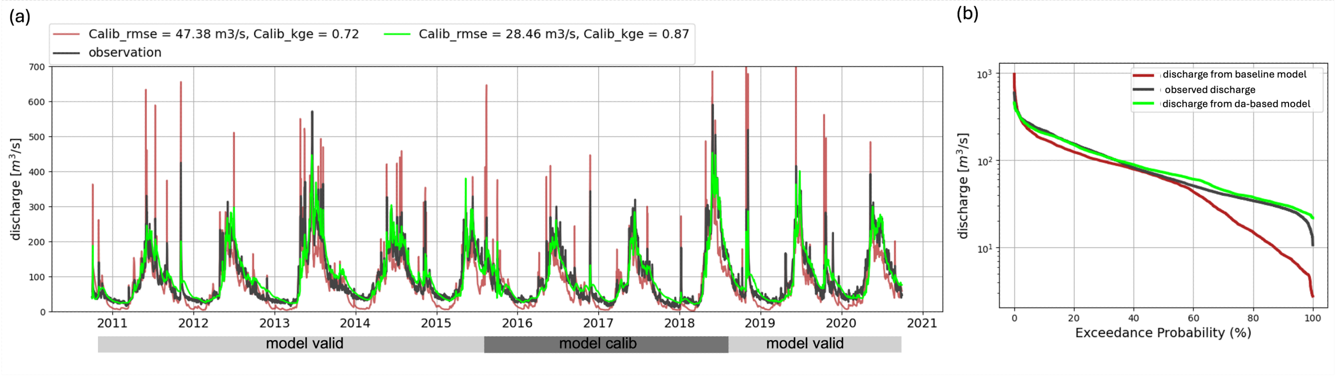

Figure 9. Simulated river discharge by the GEOframe model forced with the baseline snowfall (red) and with corrected snowfall (green). The rainfall input values in both simulations are the same. Results are shown for the calibration period (water years 2015–2018) and the validation period (remaining years from 2010 to 2020). The horizontal grey bars indicate the periods used for calibrating and validating the model parameters. (b) Flow duration curves corresponding to the simulations in panel (a), using the same color scheme.

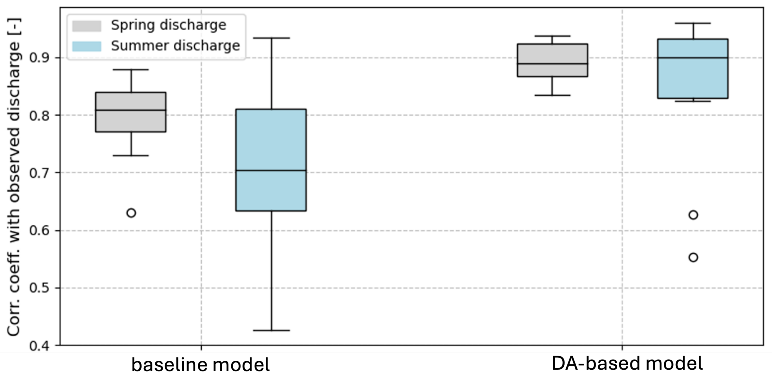

Figure 10. Correlation between observed river discharge during spring and summer (shown in grey and blue, respectively, representing the snowmelt period) and the simulations obtained from the DA-based and baseline models over the Aosta Valley catchment.

4.3 Positive implications and limitations of the proposed method

We investigated how the description of snowfall dynamics in mountainous regions can be improved by combining satellite observations with a simple numerical model, both of which are subject to uncertainty. The study addresses a critical research challenge by demonstrating how uncertainties in snowfall propagate through modeling frameworks and significantly affect estimates of snow dynamics and river discharge in regions that supply snowmelt-driven discharge to downstream areas. The validation results in this study demonstrate that the proposed framework is extendable to other regions with limited data availability. One limitation of our proposed approach for snowfall correction potentially is related to wet-snow conditions, where Sentinel-1 C-band snow-depth estimates are more uncertain. Although we only assimilated Sentinel-1 C-band data

https://doi.org/10.5194/egusphere-2026-793
Preprint. Discussion started: 17 March 2026

during storm events when the snow was dry, there remains an opportunity to better identify dry-snow conditions for assimilation into the model. Additionally, we applied a constant rainfall correction factor of 1 and only adjusted the snowfall component, meaning that total precipitation was not modified and only the snowfall portion was corrected.

5 Conclusions

In this study, a snow depth data assimilation framework was implemented to correct snow model states and improve snowfall estimation in parts of the Italian Alps, including the Aosta Valley catchment and Piemonte headwaters, which supply snowmelt-driven discharge to downstream areas. Specifically, the study explored the potential of assimilating Sentinel-1 C-band snow depth observations into the snow model within the GEOframe framework, coupled with a snow-density model.

The data assimilation process for each sub-catchment involved generating 100 particles representing correction factors for snowfall and associated snow parameters. Each particle set was then used to run the snow components of the GEOframe model. Subsequently, the average snow depth retrieved from Sentinel-1 for each subcatchment was incorporated into the assimilation process. Sentinel-1 snow depth data were assimilated only on dates following storm events between January and mid-April, when dry snow conditions are more likely and radar backscatter is more reliable. The updated weights derived from the assimilation were then used to generate the posterior distributions of snow parameters, snow depth, and snowfall. The results showed that the snowfall correction factor increases with elevation, indicating that the model increasingly underestimates snowfall at higher elevations and that associated uncertainty grows with altitude. Consequently, the corrected snowfall at higher elevations is larger than the baseline (model's estimated snowfall with α_s set to 1), particularly in the Aosta Valley catchment.

The reliability of the corrected snowfall produced by the proposed data assimilation method was evaluated using a leave-one-out approach, which indicates that the snowfall estimates from the proposed method are more accurate than those of the baseline. Corrected snowfall forcing of the GEOframe snow component improved river discharge simulations across the catchments, particularly during the snowmelt season, compared with the baseline model. In this regard, a better correlation between observed and simulated river discharge during the snowmelt season demonstrates that the corrected snowfall outperformed the baseline snowfall. River discharge–based validation was conducted exclusively over the Aosta Valley catchment, which fully coincides with the study area; only the headwater portion of the Piemonte catchment was included.

By leveraging Sentinel-1 snow depth retrievals, we improved the ability to accurately estimate river discharge and snow dynamics, particularly in snow-dominated regions. These advancements have important implications for water management, flood forecasting, and climate resilience in mountainous catchments.

Author contributions. S. A. wrote the manuscript draft, performed all analyses, and developed the code for this study. M. G. and C. H. supervised the work, provided feedback on analyses and revised the manuscript. G. R. revised the manuscript and contributed to some analyses. S. B. and R. R. contributed to revising the manuscript and provided feedback on analyses and interpretations. All authors reviewed and approved the final version.

Competing interests. The authors declare that no competing interests are present

Code and data availability. All codes and data will be made available upon request.

https://doi.org/10.5194/egusphere-2026-793
Preprint. Discussion started: 17 March 2026

References

Abera, W., Formetta, G., Borga, M., and Rigon, R.: Estimating the water budget components and their variability in a pre-alpine basin with JGrass-NewAGE., Advances in water resources, 104, 37–54, https://doi.org/http://dx.doi.org/10.1016/j.advwatres.2017.03.010, 2017.

Ashouri, H., Hsu, K. L., Sorooshian, S., Braithwaite, D. K., Knapp, K. R., Cecil, L. D., and Nelson, B. R.: PERSIANN-CDR: Daily precipitation climate data record from multisatellite observations for hydrological and climate studies., Bulletin of the American Meteorological Society, 96, 69–83, 2014.

Avanzi, F., Ercolani, G., Gabellani, S., Cremonese, E., Pogliotti, P., Filippa, G., Morra di Cella, U., Ratto, S., Stevenin, H., Cauduro, M., and et al.: Learning about precipitation orographic enhancement from snow-course data improves water-balance modeling., Hydrol. Earth Syst. Sci. Discuss., pp. 1–37, 2020.

Avanzi, F., Gabellani, S., Delogu, F., Silvestro, F., Pignone, F., Bruno, G., Pulvirenti, L., Squicciarino, G., Fiori, E., Rossi, L., Puca, S., Toniazzo, A., Giordano, P., Falzacappa, M., Ratto, S., Stevenin, H., Cardillo, A., Fioletti, M., Cazzuli, O., Cremonese, E., Morra di Cella, U., and Ferraris, L.: IT-SNOW: A snow reanalysis for Italy blending modeling, in situ data, and satellite observations (2010–2021), Earth System Science Data, 14, 5213–5238, https://doi.org/10.5194/essd-14-5213-2022, 2022.

Bancheri, M., Serafin, F., and Rigon, R.: The representation of hydrological dynamical systems using Extended Petri Nets (EPN)., Water Resources Research, 55, 8895–8921, https://doi.org/http://dx.doi.org/10.1029/2019WR025099, 2019.

Cho, E., Vuyovich, C. M., Kumar, S. V., Wrzesien, M. L., Kim, R. S., and Jacobs, J. M.: Precipitation biases and snow physics limitations drive the uncertainties in macroscale modeled snow water equivalent, Hydrology and Earth System Sciences, 26, 5721–5735, https://doi.org/10.5194/hess-26-5721-2022, 2022.

Dee, D. P., Uppala, S. M., Simmons, A. J., Berrisford, P., Poli, P., Kobayashi, S., et al.: The ERA-Interim Reanalysis: Configuration and Performance of the Data Assimilation System, Quarterly Journal of the Royal Meteorological Society, 137, 553–597, 2011.

Derksen, C., Lemmetyinen, J., Toose, P., Silis, A., Pulliainen, J., and Sturm, M.: Physical properties of arctic versus subarctic snow: Implications for high latitude passive microwave snow water equivalent retrievals., J. Geophys. Res.-Atmos., 119, 7254–7270, 2014.

Formetta, G., Kampf, S. K., David, O., and Rigon, R.: Snow water equivalent modeling components in NewAge-JGrass., Geoscientific Model Development, 7, 725–736, https://doi.org/http://dx.doi.org/10.5194/gmd-7-725-2014, 2014.

Foster, J. L., Sun, C., Walker, J. P., Kelly, R., Chang, A., Dong, J., and Powell, H.: Quantifying the uncertainty in passive microwave snow water equivalent observations,, Remote Sens. Environ., 94, 187–203, 2005.

Funk, C., Peterson, P., Landsfeld, M., and et al.: The climate hazards infrared precipitation with stations—a new environmental record for monitoring extremes., Sci Data 2, 150066, https://doi.org/https://doi.org/10.1038/sdata.2015.66, 2015.

Gelaro, R., McCarty, W., Suarez, M. J., Todling, R., Molod, A., Takacs, L., and Draper, C.: The Modern-Era Retrospective Analysis for Research and Applications, Version 2 (MERRA-2), Journal of Climate, 30, 5419–5454, 2017.

Girotto, M., Margulis, S. A., and Durand, M.: robabilistic swe reanalysis as a generalization of deterministic swe reconstruction techniques., Hydrol. Process, 28, 3875–3895, 2014.

Girotto, M., Musselman, K. N., and Essery, R. L.: Data assimilation improves estimates of climate-sensitive seasonal snow., Curr. Clim. Change Rep., 6, 81–94, 2020.

Girotto, M., Formetta, G., Azimi, S., Bachand, C., Cowherd, M., De Lannoy, G., Lievens, H., Modanesi, S., Raleigh, M., Rigon, R., and Massari, C.: Identifying snowfall elevation patterns by assimilating satellite-based snow depth retrievals., Science of The Total Environment, 906, 2024.

https://doi.org/10.5194/egusphere-2026-793
Preprint. Discussion started: 17 March 2026

Gordon, N. J., Salmond, D. J., and Smith, A. F. M.: Novel approach to nonlinear/non-Gaussian Bayesian state estimation., EE Proceedings F (Radar and Signal Processing), 140, 107–113, 1993.

Harpold, A. A., Kaplan, K. p., Klos, P. Z., Link, T., McNamara, J. P., Rajagopal, S., Schumer, P., and Steele, C. M.: Rain or snow: hydrologic processes, observations, prediction, and research needs., Hydrol. Earth Syst. Sci., 21, 1–22, 2017.

Hedrick, A., Marks, D., Havens, S., Robertson, M., Johnson, M., Sandusky, M., Marshall, H.-P., Kormos, P., Bormann, K., and Painter, T.: Direct insertion of NASA Airborne Snow Observatory-derived snow depth time series into the ISNOBAL energy balance snow model, Water Resour. Res., 54, 8045–8063, 2018.

Hersbach, H., Bell, W., Berrisford, P., Hirahara, S., Horányi, A., Muñoz-Sabater, J., and Simmons, A.: The ERA5 global reanalysis., Quarterly Journal of the Royal Meteorological Society, 146, 1999–2049, 2020.

Hou, A., Kakar, R., Neeck, S., Azarbarzin, A., C.D, K., Kojima, M., and et al.: The global precipitation measurement mission., Bulletin of the American Meteorological Society, 95, 701–722, 2014.

Leeuwen, P. V.: Particle filtering in geophysical systems, Mon. Weather Rev., 137, 4089–4114, 2009.

Lievens, H., Demuzere, M., Marshall, H. P., Reichle, R. H., Brucker, L., Brangers, I., de Rosnay, P., Dumont, M., Girotto, M., Immerzeel, W. W., and Jonas, T.: Snow depth variability in the Northern Hemisphere mountains observed from space., Nature communications, 10, 1–12, https://doi.org/https://www.nature.com/articles/s41467-019-12566-y, 2019.

Lievens, H., Brangers, I., Marshall, H. P., Jonas, T., Olefs, M., and De Lannoy, G.: Sentinel-1 snow depth retrieval at sub-kilometer resolution over the European Alps., The Cryosphere, 16, 159–177, 2022.

Lundquist, J., Abel, M. R., Gutmann, E., and Kapnick, S.: Our Skill in Modeling Mountain Rain and Snow is Bypassing the Skill of Our Observational Networks, Bulletin of the American Meteorological Society, 100, 2473–2490, 2019.

Margulis, S. A., Girotto, M., Cortés, G., and Durand, M.: A particle batch smoother approach to snow water equivalent estimation., J. Hydrometeorol., 16, 1752–1772, 2015.

Marks, D., Domingo, J., Susong, D., Link, T., and Garen, D.: A spatially distributed energy balance snowmelt model for application in mountain basins, Hydrological Processes, 13, 1935–1959, https://doi.org/10.1002/(SICI)1099-1085(199909)13:12/13<1935::AID-HYP868>3.0.CO;2-C, 1999.

Painter, T., Berisford, D., Boardman, J., Bormann, K., Deems, J., Gehrke, F., Hedrick, A., Joyce, M., Laidlaw, R., Marks, D., and et al.: The airborne snow observatory: fusion of scanning lidar, imaging spectrometer, and physically-based modeling for mapping snow water equivalent and snow albedo, Remote Sens. Environ., 184, 139–152, 2016.

Pflug, J. M., Wrzesien, M. L., Kumar, S. V., Cho, E., Arsenault, K. R., and et al: Extending the utility of space-borne snow water equivalent observations over vegetated areas with data assimilation., Hydrol. Earth Syst. Sci., 28, 631–648, 2024.

Raleigh, M. S., Livneh, B., Lapo, K., and Lundquist, J. D.: How does availability of meteorological forcing data impact physically based snowpack simulations?, Hydrol. Earth Syst. Sci., 17, 99–120, 2016.

Rott, H., Yueh, S. H., Cline, D. W., Duguay, C., Essery, R., Haas, C., Hélière, F., Kern, M., Macelloni, G., Malnes, E., and Thompson, A.: Cold regions hydrology high-resolution observatory for snow and cold land processes., P. IEEE, 98, 752–765, 2010.

Smyth, E. J., M Raleigh, M. s., and Small, E. E.: The challenges of simulating swe beneath forest canopies are reduced by data assimilation of snow depth., Water Resour. Res., 58, 2022.

Winstral, A., Magnusson, J., Schirmer, M., and Jonas, T.: The bias-detecting ensemble: a new and efficient technique for dynamically incorporating observations into physics-based, multilayer snow models., Water Resour. Res., 55, 613–631, 2019.

Yamamoto, J. K.: Correcting the Smoothing Effect of Ordinary Kriging Estimates, Mathematical Geology, 37, 69–94, https://doi.org/10.1007/s11004-005-8748-7, 2005.

Appendix A: Appendix A

https://doi.org/10.5194/egusphere-2026-793
Preprint. Discussion started: 17 March 2026

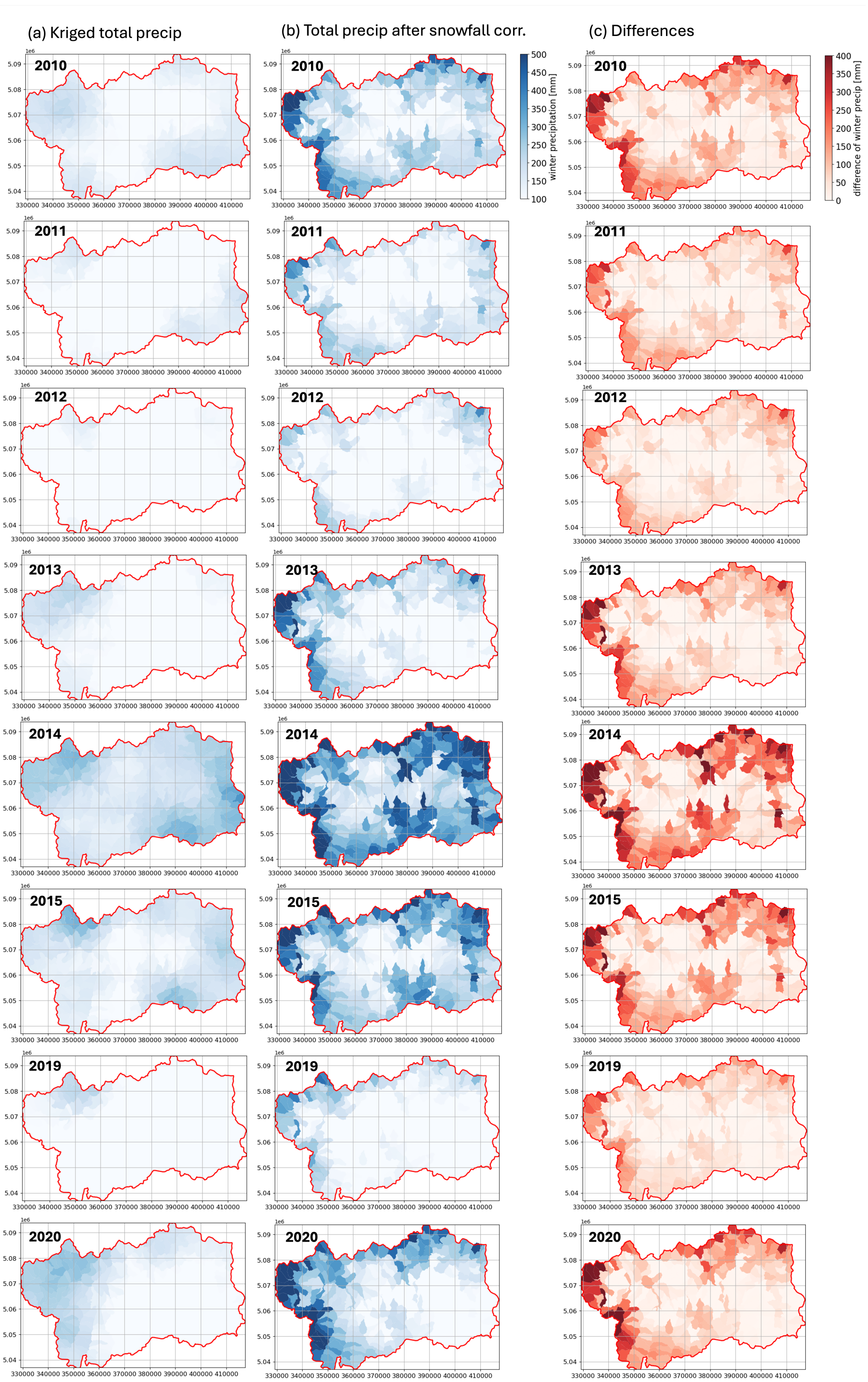

Figure A1. January–March precipitation over the Aosta Valley for different water years, based on the original snowfall (column a) and corrected snowfall via data assimilation (column b). Column (c) shows the difference between a and b, highlighting areas most affected by the correction. Higher elevations show larger changes, while the lower variations occur in the valley areas.

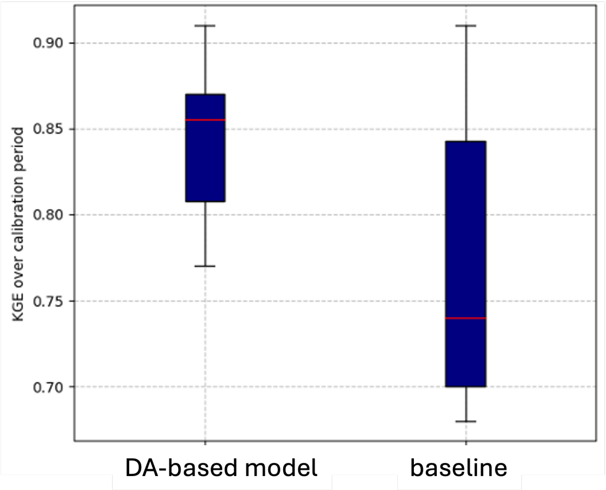

Figure A2. The variation of KGE values between observed and simulated river discharge during the calibration period across the Aosta Valley catchment.

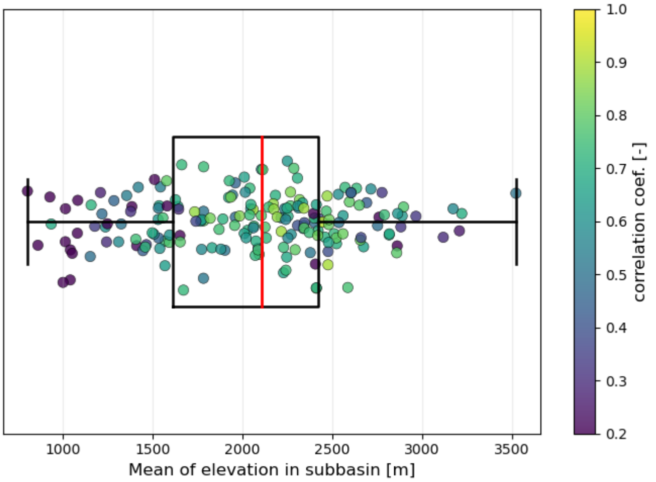

Figure A3. Correlation coefficient between the SWE time series obtained from the GEOframe model forced with corrected snowfall and the IT-SNOW data (Avanzi et al., 2022) over the study area (Aosta Valley and the headwater of Piemonte catchments).

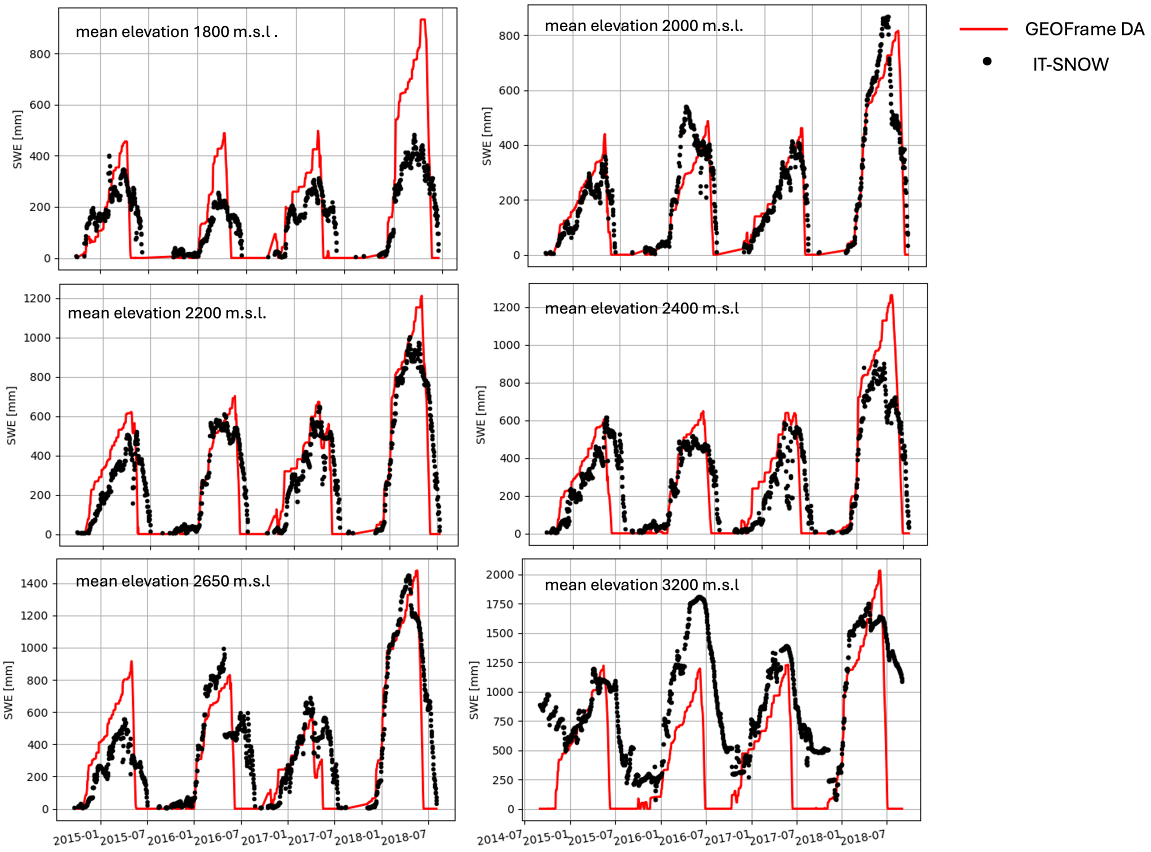

Figure A4. Comparison of SWE obtained from the GEOframe model using snowfall corrected by the proposed method with IT-SNOW datasets. The comparison is performed for subbasins with different mean elevations over the study area (Aosta Valley and the headwater of Piemonte catchments) to provide a comprehensive overview. IT-SNOW generally underestimates SWE compared to the C-band dataset. (Avanzi et al., 2022) reported that IT-SNOW underestimates snow depth relative to C-band measurements (which we used for assimilation into the model), which may explain the observed underestimation of SWE in this analysis. The overestimation of SWE by IT-SNOW in the subbasin with high elevations (e.g., 3200 m in Aosta Valley) needs further investigation.

https://doi.org/10.5194/egusphere-2026-793
Preprint. Discussion started: 17 March 2026

Table A1. Applied ranges of the GEOframe hydrological model parameters used in this study.

Parameter	**Lower Bound**	**Upper Bound**	**Description**
Precipitation parameters			
α_S	–	–	Snowfall correction factor, to be corrected during data assimilation [-]
α_r	–	–	Rainfall correction factor, considered equal to 1 [-]
Snow parameters			
meltingTemperature	-3	3	Melting temperature threshold [°C]
combinedMeltingFactor	2.5	11.6	Melting factor [mm °C^{-1} day^{-1}]
freezingFactor	0.1	0.5	Freezing factor [mm °C^{-1} day^{-1}]
radiationFactor	1.0E-5	0.01	Radiation factor (Hock model) [mm °C^{-1} day^{-1}]
α_l	0.00001	1	Snow porosity coefficient [-]
Other parameters			
kc	0.00001	2	Canopy outflow coefficient [-]
p	0.001	0.98	Free throughfall partitioning coefficient [-]
s_RootZoneMax	10	3000	Maximum root-zone water storage [mm]
g	0.1	7	Maximum percolation rate [-]
h	0.1	7	Non-linear reservoir exponent [-]
pB_soil	0.1	4.0	Soil moisture capacity spatial variability [-]
c	0.1	10	Non-linear reservoir coefficient [-]
d	0.1	10	Non-linear reservoir exponent [-]
s_RunoffMax	1	2000	Maximum runoff storage [mm]
e	0.0001	5	Non-linear reservoir coefficient [-]
f	0.1	5	Non-linear reservoir exponent [-]
s_GroundWaterMax	10	3000	Maximum groundwater storage [mm]